

# Quantum Phases of the Shastry-Sutherland Antiferromagnet

C. H. Chung and J. B. Marston

*Department of Physics, Brown University, Providence, RI 02912-1843*

Subir Sachdev

*Department of Physics, Harvard University, Cambridge MA 02138*

*and Department of Physics, Yale University, P.O. Box 208120, New Haven, CT 06520-8120*

(February 12, 2001)

We study possible paramagnetic phases of antiferromagnets on the Shastry-Sutherland lattice by a gauge-theoretic analysis of fluctuations in a theory with  $\text{Sp}(2N)$  symmetry. In addition to the familiar dimer phase, we find a confining phase with plaquette order, and a topologically ordered phase with deconfined  $S = 1/2$  spinons and helical spin correlations. The deconfined phase is contiguous to the dimer phase, and in a regime of couplings close to those found in the insulator  $\text{SrCu}_2(\text{BO}_3)_2$ . We suggest that a superconductor obtained by doping this insulator with mobile charge carriers will be an attractive candidate for observing the anomalous magnetic flux properties associated with topological order.

## I. INTRODUCTION

Much interest has recently focused on the magnetic properties of the insulator  $\text{SrCu}_2(\text{BO}_3)_2$ <sup>1,2</sup>. The low energy spin excitations in this material reside on the  $S = 1/2$  Cu ions which lie in two-dimensional layers decoupled from each other. The experiments show a clear indication of an energy gap towards spin excitations, making this one of the few known two-dimensional systems with a spin gap. Remarkably, the pattern of near-neighbor antiferromagnetic exchange couplings between the Cu ions turns out to be identical to that in a model Hamiltonian studied many years ago by Shastry and Sutherland<sup>3</sup>. These authors also showed that a simple decoupled dimer wavefunction was an exact eigenstate of this Hamiltonian, and that it was the ground state over a restricted parameter regime.

The Shastry-Sutherland antiferromagnet is sketched in Fig 1. The Hamiltonian is

$$H = J_1 \sum_{\langle ij \rangle} \mathbf{S}_i \cdot \mathbf{S}_j + J_2 \sum_{\text{diagonals}} \mathbf{S}_i \cdot \mathbf{S}_j \quad (1.1)$$

where  $\mathbf{S}_i$  are  $S = 1/2$  operators on the sites,  $i$ , of a square lattice. The exchange  $J_1 > 0$  acts along the nearest neighbor links (shown as full lines in Fig 1), while  $J_2 > 0$  acts on the diagonal links, shown as dashed in lines in Fig 1. It was established<sup>3</sup> that a simple product of singlet pairs on the diagonal links was the ground state of  $H$  for sufficiently large  $J_2/J_1$ . However, an understanding of the experiments requires a description of the excitation spectrum, and also of possible quantum phase transitions to other states at smaller  $J_2/J_1$ . These issues have been addressed in a number of recent theoretical works<sup>4-11</sup>. Many of these studies<sup>4,6-8</sup> involve numerical analyses based upon large-order series expansions departing from various decoupled cluster states. Quantum Monte Carlo simulations have, in principle, a smaller

bias due to the choice of an initial state, and can be extended to much large system sizes; however, simulations of  $H$  suffer from a sign problem, and so such studies have not been possible. An analytic mean-field approach has also been undertaken by Albrecht and Mila<sup>5</sup>: results were obtained mainly for the magnetically ordered states, and the various distinct paramagnetic states were not distinguished.

Quite apart from determining the ground states of the specific Hamiltonian  $H$ , it is also of interest to determine the phases of models which are “near” the parameter space of  $H$ . This is in the hope that future experiments may succeed in deforming the insulator  $\text{SrCu}_2(\text{BO}_3)_2$  by substitutional doping (which can induce mobile carriers), or by the application of hydrostatic pressure. Doping the antiferromagnetic insulator  $\text{La}_2\text{CuO}_4$  led to the discovery of high temperature superconductivity: related phenomena may be expected here, although, as we shall argue later, the presence of strong frustration in the parent insulator  $\text{SrCu}_2(\text{BO}_3)_2$  may lead to profound differences in the nature of a possible superconducting ground state.

This paper will examine a generalization of  $H$  to  $\text{Sp}(2N)$  symmetry ( $\text{SU}(2) \cong \text{Sp}(2)$ ) and describe the properties of the large  $N$  limit. Some of the phases obtained in such a large  $N$  limit may not actually appear in the phase diagram of the  $\text{SU}(2)$  model  $H$ —nevertheless, as we have just argued, the phases may still be of relevance to physical systems whose microscopic Hamiltonians are near the parameter space of  $H$ . Such an approach has been fruitfully applied to a number of other frustrated quantum antiferromagnets in previous work<sup>12-16</sup>. The method leads to an unbiased selection of possible ground states in the large  $N$  limit, both with and without broken spin rotation symmetry. Moreover, a gauge-theoretic description of the fluctuations about the mean-field solution allows a systematic and reliable assessment of the stability of the various ground states, along with a description of the dynamics of the excita-

tions.

The  $\text{Sp}(2N)$  generalization of  $H$  is defined by introducing canonical Bose creation operators  $b_{i\alpha}^\dagger$  on every site  $i$ , with  $\alpha = 1 \dots 2N$  a  $\text{Sp}(2N)$  index. The allowed states in the Hilbert space satisfy the constraint

$$b_{i\alpha}^\dagger b_i^\alpha = 2NS \quad (1.2)$$

on every site  $i$  (we follow the convention of summing over all repeated  $\text{Sp}(2N)$  indices); the right hand side of (1.2) must be a positive integer, the values of  $S$  are constrained accordingly—for the physical case,  $N = 1$ ,  $S$  must take half-integral values, as expected. The Hamiltonian is

$$H = -\frac{J_1}{2N} \sum_{\langle ij \rangle} \left( \mathcal{J}^{\alpha\beta} b_{i\alpha}^\dagger b_{j\beta}^\dagger \right) \left( \mathcal{J}_{\gamma\delta} b_i^\gamma b_j^\delta \right) - \frac{J_2}{2N} \sum_{\text{diagonals}} \left( \mathcal{J}^{\alpha\beta} b_{i\alpha}^\dagger b_{j\beta}^\dagger \right) \left( \mathcal{J}_{\gamma\delta} b_i^\gamma b_j^\delta \right) \quad (1.3)$$

where  $\mathcal{J}^{\alpha\beta} = \mathcal{J}_{\alpha\beta} = -\mathcal{J}_{\beta\alpha}$  is the generalization of the antisymmetric  $\varepsilon$  tensor of  $\text{SU}(2)$  (*i.e.*  $\mathcal{J}$  contains  $N$  copies of  $\varepsilon$  along its center block diagonal, and vanishes elsewhere).

The large  $N$  analysis of a large class of models, of which  $H$  is a member, was described with some generality in Section II of Ref. 15. We will follow the same method here, and so will dispense with the details of the computation. The resulting mean-field phase diagram is shown in Fig 3 as a function of  $J_2/J_1$  and  $1/S$  (in the large  $N$  limit,  $S$  becomes a continuous real variable). The positions of the various phase boundaries are not expected to be quantitatively accurate for the physical  $N = 1$  case. However, the general topology of the phase diagram, the nature of the phases and their excitations, and the critical properties of the quantum phase transitions can be reliably described using Fig 3 as a starting point.

The properties of all the phases in Fig 3 will be discussed in detail in Section II. Here we highlight our main new results.

One of the paramagnetic phases has short-range equal-time spin correlations peaked at the wavevector  $(\pi, \pi)$ . [We denote this phase  $(\pi, \pi)$  short-range ordered (SRO) in Fig 3; here we are placing the sites on the vertices of a regular square lattice as in Fig 1, and measuring wavevectors in units of  $1/(\text{nearest neighbor spacing})$ . In the experimental  $\text{SrCu}_2(\text{BO}_3)_2$  system, the positions of the sites is different, and there will be a corresponding transformation in the wavevector dependence of observables.] At the mean field level, this phase is identical to that found earlier<sup>19,20</sup> on the square lattice with  $J_2 = 0$ . However, we will show here that a difference does emerge upon consideration of fluctuations. For  $J_2 = 0$ , it was shown<sup>19,20</sup> that Berry phases associated with hedgehog-instantons led to columnar spin-Peierls order in the  $(\pi, \pi)$  SRO phase. Here we show that a closely related analysis for the Shastry-Sutherland lattice leads instead to

“plaquette” order in this phase. Just such a phase was considered recently by Koga and Kawakami<sup>8</sup>.

Our other new results are also associated with a paramagnetic phase. This phase is denoted  $(\pi, q)$  SRO in Fig 3 and is obtained by a destroying the long-range magnetic order in a helically ordered phase. Equal-time spin correlations show short-range incommensurate order, and the spin structure factor is peaked at the incommensurate wavevector  $(\pi, q)$  (the value of  $q$  varies continuously as a function of  $J_2/J_1$ ). As in previous incommensurate SRO phases found on frustrated square lattice models<sup>12,14</sup>, we argue that the excitations above the ground state are *deconfined spinons* which carry spin  $S = 1/2$  (for  $\text{SU}(2)$ ). Also as in previous work<sup>12,14</sup>, the quantum phase transition between this phase and the  $(\pi, \pi)$  SRO (plaquette) phase (Fig 3) is described by theory of a charge 2 Higgs scalar coupled to a compact  $U(1)$  gauge field; the deconfinement transition is associated with the condensation of the Higgs field, and the critical properties are those of a  $Z_2$  gauge theory<sup>21,12–14,22–24</sup>. We will also consider here the transition between the deconfined phase and the dimer phase: by a somewhat different analysis, we will show that this transition also reduces to a  $Z_2$  gauge theory description.

## II. MEAN FIELD PHASE DIAGRAM

As discussed in Section II of Ref. 15, a key quantity determining the nature of the phases is a complex, directed, link field  $Q_{ij} = -Q_{ji}$ . Operationally, this field is introduced to decouple the quartic boson interactions in  $H$  by a Hubbard-Stratonovich transformation. After this decoupling, the effective action contains the terms

$$\mathcal{S} = \int d\tau \sum_{i>j} \frac{J_{ij}}{2} \left[ N|Q_{ij}|^2 - Q_{ij} \mathcal{J}_{\alpha\beta} b_i^\alpha b_j^\beta + \text{H.c.} \right] + \dots, \quad (2.1)$$

where  $\tau$  is imaginary time,  $J_{ij} = J_1$  ( $J_{ij} = J_2$ ) on the horizontal/vertical (diagonal) links, and the ellipses represent standard terms which impose the canonical boson commutation relations and the constraint (1.2). It is also clear from the structure of  $\mathcal{S}$  that the average value of  $Q_{ij}$  satisfies

$$\langle Q_{ij} \rangle = \frac{1}{N} \left\langle \mathcal{J}^{\alpha\beta} b_{i\alpha}^\dagger b_{j\beta}^\dagger \right\rangle. \quad (2.2)$$

For larger values of  $S$ , the dynamics of  $\mathcal{S}$  requires condensation of the  $b_i^\alpha$  bosons, and hence a non-zero value of

$$x_i^\alpha = \langle b_i^\alpha \rangle; \quad (2.3)$$

such phases break the spin rotation symmetry, and have magnetic long-range order. As described in Ref 15, we optimized the ground state energy with respect to variations in  $\langle Q_{ij} \rangle$  and  $x_i^\alpha$  for different values of  $J_2/J_1$  and  $S$ .

The four-site unit cell of the Shastry-Sutherland lattice, depicted in Fig 2, has 10 different  $Q_{ij}$  fields. Care must be taken to identify gauge-equivalent configurations. We find that each saddle point may be described by purely real  $\langle Q_{ij} \rangle$ . The resulting phase diagram is shown in Fig 3. We describe the phases in turn in the following subsections, considering first the magnetically ordered phases with  $x_i^\alpha \neq 0$  in Subsection II A, and then the paramagnetic phases in Subsection II B.

## A. Magnetically ordered phases

### 1. Néel $(\pi, \pi)$ LRO state

This is the familiar long-range ordered (LRO) state in which  $\langle \mathbf{S}_i \rangle$  is collinearly polarized in opposite directions on two checkerboard sublattices. It is known to be the ground state of  $H$  for  $J_2 = 0$ ,  $S = 1/2$  in the physical  $N = 1$  limit. A gauge may be chosen in which the expectation values of link variables,  $\langle Q_{ij} \rangle$ , are nonzero and equal on the horizontal and vertical links, while the expectation values on the diagonal links are zero. In the notation of Fig 2 then  $Q_i = P_i$  ( $i = 1, 2, 3, 4$ ) and  $R_1 = R_2 = 0$ .

### 2. Helical $(\pi, q)$ and $(q, \pi)$ LRO states

This phase is characterized by non-zero values of  $\langle Q_{ij} \rangle$  on the horizontal, vertical and diagonal links. A gauge choice sets all the  $Q_i$  equal to each other, and similarly for the  $P_i$ ; in the appendix we present an argument which shows the values of the  $P_i$  and  $Q_i$  are also equal to each other. There are two gauge non-equivalent choices for the values of  $R_{1,2}$ : one state has  $R_1 = R_2$  and the other  $R_1 = -R_2$ . The two states are interchanged under a  $90^\circ$  rotation, and correspond to spirals ordered in the horizontal or vertical directions. At large values of the spin, this phase appears at  $J_2 > J_1$ , in accord with the classical calculation of Shastry and Sutherland<sup>3</sup>. Equal-time spin correlations exhibit long-range incommensurate order, and the spin structure factor peaks at the incommensurate wavevectors  $(\pi, q)$  or  $(q, \pi)$  with the value of  $q$  varying continuously as a function of  $J_2/J_1$ . This state also appears in the studies of Refs 5,10.

## B. Paramagnetic phases

In this subsection we discuss the three phases for which  $x_i^\alpha = 0$ . As a consequence, spin rotation symmetry is preserved and only spin SRO arises; however there may be ordering in other singlet order parameters.

### 1. Dimer state

This is the exact  $SU(2)$  eigenstate of decoupled singlet pairs found by Shastry and Sutherland<sup>3</sup>. In the large  $N$  limit, this corresponds to a saddle point at which the  $\langle Q_{ij} \rangle$  are non-zero only on the diagonal links:  $R_1 = R_2 \neq 0$  and  $Q_i = P_i = 0$ . Note that the  $b_i^\alpha$  boson are spatially decoupled at such a saddle point: each  $b_i^\alpha$  can only hop across a single diagonal link. This simplifies analysis of fluctuations about the saddle point in or near the dimer state, as will be discussed in Section IV. At higher orders in  $1/N$ , the  $b_i^\alpha$  can indeed hop through the entire lattice; we expect that the lowest lying excitation will be a  $S = 1$  spin triplet<sup>4</sup> (for  $SU(2)$ ), consisting of a confined pair of the  $b_i^\alpha$  bosons.

### 2. $(\pi, \pi)$ SRO

This state is obtained by quantum-disordering the Néel state of Subsection II A 1, and the expectation values of  $Q_{ij}$  have the same structure as those in Subsection II A 1. As has been discussed in some detail in Refs 19,20, the quantum fluctuations in this phase are described by a compact  $U(1)$  gauge theory. Such a theory is always confining, and thus the  $b_i^\alpha$  bosons again bind to yield a  $S = 1$  quasiparticle above a spin gap. There is also an interesting structure in the spin-singlet sector: this is considered in Subsection III where it is demonstrated that at finite  $N$  this phase has “plaquette” order.

### 3. $(\pi, q)$ and $(q, \pi)$ SRO

In this phase  $\langle Q_{ij} \rangle$  are non-zero on the diagonal, horizontal and vertical links, like the helical  $(\pi, q)$  LRO phase of Subsection II A 2. Again there are two gauge non-equivalent configurations, corresponding to the choices  $R_1 = R_2$  with  $Q_i = Q < P_i = P$  [the  $(\pi, q)$  phase], and  $R_1 = -R_2$  with  $Q_i = Q > P_i = P$  [the  $(q, \pi)$  phase]. Thus all of the horizontal  $Q_i$  fields acquire the same expectation value, but unlike in the helical LRO phase, this value differs slightly from that of the vertical  $P_i$  fields; the difference is only on the order of a part in ten thousand. The state is a spin-singlet and there is a gap to all spin excitations. Nevertheless, the symmetry of  $90^\circ$  rotations between the vertical and horizontal directions is broken—this would now be apparent in various spin-singlet observables like the bond exchange energies or the bond-charge densities. This phase may therefore be viewed as a spin-singlet “nematic” as only rotational symmetry is broken. The choice of a vertical or horizontal spatial polarization in the nematic order leads to a two-fold degeneracy in the ground state. The state also has “topological” order<sup>25,26,12,24,27,28</sup>, and this would lead to an additional four-fold degeneracy in a torus geometry. Unlike the commensurate SRO phases, the spinons are

deconfined. We describe the deconfinement transition below in Section IV. The spinon dispersion has its minima at momentum  $(\pi/2, q/2)$  or  $(q/2, \pi/2)$ . Although this phase is realized only for  $S < 1/2$  in the large  $N$  limit, it seems possible that in the physical limit  $N = 1$  it could extend up to  $S = 1/2$  for a narrow range of  $J_2/J_1$ . Similar behavior was found in a study of the  $\text{Sp}(2N)$  Heisenberg antiferromagnet on the anisotropic triangular lattice<sup>16</sup>. It would be interesting to search for this phase using numerical methods.

We conclude this section by briefly comparing our results to other published calculations. For  $S = 1/2$  we find that the transition between Néel and Helical LRO phases is continuous, occurring at  $J_2/J_1 \approx 1.02$ , close to the value of 1.1 found by Albrecht and Mila<sup>5</sup>, who also report a continuous transition. Also in agreement with Albrecht and Mila, we find that the transition between the Helical LRO and Dimer SRO phase is first order, but occurs at  $J_2/J_1 \approx 2.7$  instead of 1.65. Carpentier and Balents<sup>10</sup> also found a helical LRO phase, but presented arguments that an intermediate phase may exist between the helical LRO and dimer phases: our  $(\pi, q)$  SRO state is precisely such a phase. Koga and Kawakami<sup>8</sup> employed a series expansion to find, for  $S = 1/2$ , a plaquette phase which intervenes between the Néel and dimer phases. As shown below, the  $(\pi, \pi)$  SRO phase acquires plaquette order at finite  $N$ , but as can be seen in Fig 3, at large  $N$  this phase only occurs for  $S < 1/5$ . If finite  $N$  fluctuations push the phase boundary up to  $S = 1/2$  then the following sequence of phases would occur as  $J_2/(J_1 + J_2)$  increases from 0 to 1: Néel, Plaquette  $(\pi, \pi)$  SRO,  $(\pi, q)$  SRO, and finally Dimer SRO.

### III. PLAQUETTE ORDER IN THE COMMENSURATE PARAMAGNET

This section will discuss the fate of the spin singlet sector upon including fluctuations about the mean-field in the  $(\pi, \pi)$  SRO state. The results below are a straightforward generalization of those obtained in Refs 19,20 for the square lattice antiferromagnet. We will only consider the case where  $2SN$  is an odd integer (for the physical  $SU(2)$  case, this means that  $S$  is half an odd integer); the generalization to other values of  $S$  follows as in earlier work.

In the present large  $N$  approach, regular perturbative corrections order by order in  $1/N$  do not qualitatively modify the nature of the mean-field ground state. However, singular effects do appear<sup>19,20</sup> upon considering the consequences of ‘hedgehog’ like instanton tunneling events and their Berry phases. Such a calculation is technically involved, and a somewhat more transparent discussion of essentially the same physics emerges from studying the “quantum dimer” model<sup>25</sup> (see Appendix A of Ref 20 for a discussion of the equivalence between the instanton physics of the large  $N$  expansion and dual

representations of the quantum dimer model). Here we shall follow the treatment of Ref 29.

The quantum dimer model represents the Hilbert space of low-lying singlet excitations by assuming that it can be mapped onto states represented by a near-neighbor singlet bond (‘dimers’) covering of the lattice. In the present  $(\pi, \pi)$  SRO phase, we need only take dimers connecting nearest neighbor sites on horizontal and vertical links. The dimers along the diagonal links are assumed to occur only rarely in this phase: they can therefore be integrated out, and serve mainly to modify the effective Hamiltonian in the space of horizontal and vertical dimers. Indeed, the most important consequence of this procedure is apparent from a glance at Fig 1: the diagonal dimers divide the plaquettes of the square lattice into two classes, those with and without diagonal links across them, and we expect dimer resonance terms around these plaquettes to have distinct matrix elements (see Fig 4). This distinction will be the only difference from earlier analyses<sup>19,20</sup>, and we will show that it is sufficient to lead to plaquette order in the  $(\pi, \pi)$  SRO phase.

Our results emerge from an analysis of the ‘height’ representation of the quantum dimer model<sup>20,30,31,29,28</sup>. There is a rigorous, one-to-one mapping between the set of coverings of the square lattice with nearest-neighbor horizontal and vertical dimers, and the configurations of an interface of heights,  $h_a$ , defined on the sites,  $a$ , of the dual square lattice (we identify two interfaces as equivalent if they are related by a uniform translation  $h_a \rightarrow h_a + p$ , where  $p$  is any integer). The values of  $h_a$  are restricted to

$$h_a = n_a + \zeta_a \quad (3.1)$$

where  $n_a$  is an integer which fluctuates from site to site, and  $\zeta_a$  is a fixed fractional offset which takes the values  $0, 1/4, 1/2, 3/4$  on four dual sublattices,  $X, Y, Z, W$ , as shown in Fig 5. We further restrict the  $h_a$  to satisfy  $|h_a - h_b| < 1$  for any pair of nearest-neighbor sites  $a, b$ . We can now specify the connection between the height model and the dimer coverings. Examine the value of  $|h_a - h_b|$  for every nearest neighbor pair, and if  $|h_a - h_b| > 1/2$ , place a dimer on link shared by the plaquettes of the direct lattice around  $a$  and  $b$ . It is not difficult to see that a consequence of our choice of the  $\zeta_a$  offsets is that dimers so obtained will form a close-packed covering of the lattice. Examples of the relationship between the height values and dimer coverings are shown in Fig 4.

We can now use general symmetry considerations to write down an effective action for the height degrees of freedom. As is standard in theories of interface models, we promote discrete heights  $h_a$ , in (3.1), to continuous real variables  $\chi_a$  by the Poisson summation formula, and “soften” the constraints to periodic cosine potentials which have minima at the values  $\chi_a = h_a$  which obey (3.1). In this manner we obtain the action

$$\mathcal{S}_\chi = \int d\tau \left[ \frac{K}{2} \sum_{\langle ab \rangle} (\chi_a - \chi_b)^2 + \sum_a \left\{ \frac{K_\tau}{2} (\partial_\tau \chi_a)^2 - y_a \cos(2\pi(\chi_a - \zeta_a)) \right\} \right], \quad (3.2)$$

where the sum over  $\langle ab \rangle$  extends over nearest neighbor sites, and  $K$  is the stiffness towards spatial fluctuations of the interface height. The corresponding stiffness towards time-dependent fluctuations is  $K_\tau$ , and, for simplicity, we have taken its value  $a$  independent. The symmetry of the lattice requires that the strength of the periodic potential take two possible values,  $y_a = y_1$  or  $y_a = y_2$  depending upon whether the plaquette  $a$  has a diagonal  $J_2$  link across it or not. This is the sole distinction from the analysis of the square lattice antiferromagnet in Ref 20, which had  $y_1 = y_2$ .

The fundamental property of interface models in 2+1 dimensions, like  $\mathcal{S}_\chi$ , is that they are always in a smooth phase. This means that the symmetry of height translations is always broken, and  $\langle \chi_a \rangle = \langle h_a \rangle$  has some definite value across the entire system. As was argued in Refs 19,20, any such definite value necessarily breaks the lattice symmetry of the underlying antiferromagnet, and will lead here to plaquette order.

With the assumption of a smooth interface, the optimal interface configurations can be determined by a simple minimization of  $\mathcal{S}_\chi$  by a set of time-independent values of  $\chi_a$ . We allow for distinct expectation values,  $\chi_W, \chi_X, \chi_Y$ , and  $\chi_Z$  on the four dual sublattices. Then the problem reduces to the minimization of the following energy as a function of these four real variables:

$$E_\chi = K \left[ (\chi_X - \chi_W)^2 + (\chi_W - \chi_Y)^2 + (\chi_Y - \chi_Z)^2 + (\chi_Z - \chi_X)^2 - y_1 [\cos(2\pi\chi_W) - \cos(2\pi\chi_Y)] - y_2 [\sin(2\pi\chi_X) - \sin(2\pi\chi_Z)] \right] \quad (3.3)$$

This minimization is a straightforward, but somewhat tedious, computation. The present analysis is valid only for small  $y_1, y_2$ , and so we analytically determine the minima in power series in  $y_{1,2}$ . We define

$$\begin{aligned} \chi_W &= \chi_1 + \chi_2 + \chi_3 \\ \chi_X &= \chi_1 - \chi_2 + \chi_3 \\ \chi_Y &= \chi_1 + \chi_2 - \chi_3 \\ \chi_Z &= \chi_1 - \chi_2 - \chi_3. \end{aligned} \quad (3.4)$$

We find that at the saddle points of  $E_\chi$ ,

$$\begin{aligned} \chi_2 &= \frac{\pi^3(y_1^2 + y_2^2)}{16K^2} \sin(4\pi\chi_1) + \mathcal{O}(y_{1,2}^4) \\ \chi_3 &= -\frac{\pi y_1}{2K} \sin(2\pi\chi_1) + \mathcal{O}(y_{1,2}^3) \\ \chi_4 &= \frac{\pi y_2}{2K} \cos(2\pi\chi_1) + \mathcal{O}(y_{1,2}^3). \end{aligned} \quad (3.5)$$

The average interface height,  $\chi_1$ , is determined by the minimization of

$$E_\chi = E_0 + A \cos(4\pi\chi_1) + B \cos(8\pi\chi_1) + \dots, \quad (3.6)$$

where  $E_0$  is an uninteresting constant independent of  $\chi_1$ ,

$$\begin{aligned} A &= \frac{\pi^2(y_1^2 - y_2^2)}{2K} - \frac{\pi^6(y_1^4 - y_2^4)}{6K^3} \\ B &= \frac{\pi^6(7y_1^4 + 6y_1^2y_2^2 + 7y_2^4)}{96K^3}, \end{aligned} \quad (3.7)$$

and all omitted terms are of order  $y_{1,2}^6$  or higher (in obtaining the results in (3.7) we had to include terms in (3.5) which are one order higher than those shown). Note that the square lattice antiferromagnet, with  $y_1 = y_2$ , has  $A = 0$ .

We now have to minimize (3.6) to determine  $\chi_1$ . Then from (3.5) we know  $\chi_{2,3,4}$ , and hence the configuration of the interface heights. Then, from the connection between  $|h_a - h_b|$  and the corresponding dimer occupation numbers, we can determine the pattern of the distribution probabilities of the spin singlet bonds in the original antiferromagnet. It is a simple exercise to determine the minima of (3.6) for different values of  $A$  and  $B$ ; the resulting phase diagram is shown in Fig 6, and we now list the various minima and the associated ground states of the antiferromagnet.

(i)  $A \geq 0, B \leq A/4$ : There are degenerate minima at  $\chi_1 = 1/4, 3/4$ . The system spontaneously breaks a translational symmetry by choosing one of these minima. With the mappings above, it is easy to see that these are the plaquette states, one of which is depicted in Fig 6.

(ii)  $A \leq 0, B \leq -A/4$ : Now the two equivalent minima are  $\chi_1 = 0, 1/2$ . These also correspond to plaquette states as above, but the chosen plaquettes are now around half of those containing diagonal links (see Fig 6).

(iii) The remaining values of  $A$  and  $B$  have four degenerate minima at  $\chi_1 = 1/4 \pm \vartheta, 3/4 \pm \vartheta$ , where  $0 < \vartheta < 1/4$  varies continuously as a function of  $A/B$ . These states have spin-Peierls order of the type shown in Fig 6: the links are divided into four columnar sets, with each set having a different value of  $\langle \mathbf{S}_i \cdot \mathbf{S}_j \rangle$  on its links. This state interpolates between the plaquette state in (i) as  $\vartheta \rightarrow 0$  and that in (ii) as  $\vartheta \rightarrow 1/4$ .

The present analysis is for small  $y_1$ , and so, from (3.7) we should assume that  $B \ll |A|$ . Furthermore, the presence of the frustrating  $J_2$  interaction on half the plaquettes means that the hedgehog tunneling events are more likely to be centered on these plaquettes. Using the mapping of such events to the model (3.2), we expect that  $y_1 > y_2$ . From (3.7) we therefore conclude that the most likely possibility for the ground state is that in (i) above. The same state has also been considered in Ref 8.

We conclude this section with a few comments on the  $(\pi, \pi)$  SRO phase of the antiferromagnet with full square lattice symmetry, in which there is a diagonal  $J_2$  exchange between every pair of next-nearest-neighbor sites.

Recent numerical work on such an antiferromagnet<sup>32,18</sup> has found evidence for spin-Peierls ordering with the same spatial structure as in (iii) above for the Shastry-Sutherland antiferromagnet. However, we noted earlier that the square lattice symmetry implies that  $A = 0$ : for this value,  $\vartheta = 1/8$ , and the spin-Peierls state of (iii) has a larger symmetry (two of the four sets of columnar links are equal to each other), and becomes equivalent to the ordering discussed in Refs 19,20. To obtain  $\vartheta \neq 1/8$ , and so a ground state with the symmetry of that in Fig 6, we need to add to  $E_\chi$  a higher order term  $C \cos(16\pi\chi)$ : then there can be an *eight*-fold degenerate ground state, with  $\vartheta$  and  $1/4 - \vartheta$  equivalent to each other. This is the state that appears to have been found in Refs 32,18.

Note also that for the square lattice case, the  $B < 0$ ,  $A = 0$  solution has the four plaquette states degenerate with each other<sup>29</sup>.

#### IV. DECONFINEMENT TRANSITION OF THE DIMER PHASE

The deconfined, “spin-liquid”,  $(\pi, q)$  SRO phase in Fig 3 is flanked on both sides by confining paramagnetic phases, the plaquette and the dimer phases.

As we indicated Section I, the deconfinement-confinement quantum phase transition from the  $(\pi, q)$  SRO phase to the plaquette phase can be described in a theory essentially identical to that considered previously for frustrated square lattice antiferromagnets<sup>12,14</sup>. At the mean-field level, the transition is signaled by the onset of non-zero expectation values of  $Q_{ij}$  on the diagonal links: we will denote these diagonal  $Q_{ij}$  as  $Q_{ij}^d$ . Upon considering fluctuations, we find that the  $Q_{ij}^d$  constitute a charge 2 Higgs field in a compact  $U(1)$  gauge theory, and the deconfinement-confinement transition is that in a  $Z_2$  gauge theory<sup>21,12–14,22–24</sup>.

This section will consider the second deconfinement-confinement transition in Fig 3, between the dimer and  $(\pi, q)$  SRO phases in more detail. We will see that this is also described by a  $Z_2$  gauge theory, and the emergence of the  $Z_2$  gauge symmetry can be described in a somewhat more transparent manner.

As noted in Section IIB 1, the dimer phase is characterized by non-zero expectation values of the diagonal  $Q_{ij}^d$  links. These links are all decoupled from each other, and this leads to a simple, local structure in the effective action for the fluctuations. The transition to the deconfined phase is now signaled by the onset of non-zero expectation values of the  $Q_{ij}$  on the horizontal and vertical links, and we will denote these by  $Q_{ij}^h$  and  $Q_{ij}^v$  respectively. Near the phase boundary, we need only consider the structure of the effective action as a functional of the  $Q_{ij}^{h,v}$  after all other degrees of freedom have been integrated out.

The simplest terms in the effective action arise from the on-site propagation of the  $b_i^\alpha$  on the site  $i$  in imaginary

time. Integrating out the  $b_i^\alpha$  in powers of the  $Q_{ij}^{h,v}$ , the lowest order terms have the form

$$\mathcal{S}_1 = \int d\tau \left[ c_1 \sum_{\langle ij \rangle} |Q_{ij}^{h,v}|^2 + c_2 \sum_{\square} \{ Q_{12}^h Q_{23}^{v*} Q_{34}^h Q_{41}^{v*} + \text{H.c.} \} + \dots \right] \quad (4.1)$$

where  $c_1, c_2$  are constants, the first sum is over nearest neighbor links, and the second sum is over plaquettes, with the sites labeled as in Fig 7. A crucial property of  $\mathcal{S}_1$  is that all terms are invariant under a local  $U(1)$  gauge transformation

$$Q_{ij}^{h,v} \rightarrow Q_{ij}^{h,v} e^{i(\phi_i + \phi_j)}, \quad (4.2)$$

where the phase  $\phi_i$  can take arbitrary distinct values on the sites  $i$ .

We have so far not made use of the fact that the nonzero value of  $\langle Q_{ij}^d \rangle$  allows the  $b_i^\alpha$  bosons to hop across a single diagonal link. Such hopping processes will induce a large number of additional terms between the  $Q_{ij}^{h,v}$ . We will now write down the structure of all such terms which appear at fourth order in the  $Q_{ij}^{h,v}$ . It is convenient to group these terms into sets associated with links emanating from a given plaquette which does not have a diagonal dimer across it: one such plaquette is that with the sites 1,2,3,4 in Fig 7, and we now write down all four-link terms in which every link has at least one site on the central plaquette. It is not difficult to see that all other four-link terms can be obtained by a simple translation of these terms to other plaquettes. The terms are

$$\begin{aligned} \mathcal{S}_2 = \int d\tau \left[ c_3 \left\{ Q_{51}^h Q_{26}^v Q_{32}^{v*} Q_{43}^h - Q_{26}^v Q_{37}^h Q_{43}^{h*} Q_{41}^v \right. \right. \\ \left. \left. + Q_{37}^h Q_{84}^v Q_{41}^{v*} Q_{12}^h - Q_{84}^v Q_{51}^h Q_{12}^{h*} Q_{32}^v + c.c. \right\} \right. \\ \left. + c_4 \left\{ Q_{51}^h Q_{26}^v Q_{12}^{h*} Q_{41}^v - Q_{26}^v Q_{37}^h Q_{32}^{v*} Q_{12}^h \right. \right. \\ \left. \left. + Q_{37}^h Q_{84}^v Q_{43}^{h*} Q_{32}^v - Q_{84}^v Q_{51}^h Q_{41}^{v*} Q_{43}^h + c.c. \right\} \right. \\ \left. - c_5 \left\{ Q_{51}^h Q_{12}^{h*} Q_{37}^{h*} Q_{43}^h + Q_{26}^v Q_{32}^{v*} Q_{84}^{v*} Q_{41}^v + c.c. \right\} \right. \\ \left. + c_6 \left\{ Q_{51}^h Q_{26}^v Q_{37}^h Q_{84}^v + c.c. \right\} \right]. \quad (4.3) \end{aligned}$$

Clearly, (4.3) is not invariant under (4.2). However, a residual  $Z_2$  gauge symmetry does survive. We see that (4.1, 4.3), and all other allowed terms, are invariant under

$$Q_{ij}^{h,v} \rightarrow Q_{ij}^{h,v} \eta_i \eta_j \quad (4.4)$$

where  $\eta_i = \pm 1$  performs the gauge transformation. However, it is *not* possible to choose the  $\eta_i$  independently on every site: it is easy to see that we need the additional constraint

$$\begin{aligned} \eta_i = \eta_j \text{ whenever } i \text{ and } j \\ \text{are separated by a diagonal link.} \end{aligned} \quad (4.5)$$

So the  $Z_2$  gauge degree of freedom is halved from that present on the original square lattice.

To place the  $Z_2$  gauge theory in a more conventional form, it is useful to introduce a slightly different parameterization of the degrees of freedom. First, we neglect all amplitude and phase fluctuations and replace all the  $Q_{ij}$  by discrete Ising variables taken only the values  $\pm 1$ . Then we choose to represent all the  $Q_{ij}^h$  as Ising gauge fields,  $\sigma$ , while all the  $Q_{ij}^v$  are written as products of  $\sigma$  and a second Ising spin field,  $\mu$ ; thus:

$$\begin{aligned} Q^h &\sim \sigma \\ Q^v &\sim \sigma\mu. \end{aligned} \quad (4.6)$$

This is shown more explicitly in Fig 7. Notice that each pair of horizontal and vertical links that form a triangle with a single diagonal link share the same Ising gauge field  $\sigma$ . This choice is a consequence of the constraint (4.5)—as a result, all the  $\mu$  fields are *invariant* under the gauge transformation generated by the  $\eta_i$ , while the  $\sigma$ 's transform like conventional Ising gauge fields. This is also evident from the structure of the effective action obtained by substituting the parameterization in (4.6) and Fig 7 into the effective action in (4.1, 4.3); for the terms displayed in (4.1, 4.3) we obtain:

$$\begin{aligned} \mathcal{S}_3 = \int d\tau \left[ \tilde{c}_2 \sigma_1 \sigma_2 \sigma_3 \sigma_4 \mu_2 \mu_4 \right. \\ \left. + \tilde{c}_3 \sigma_1 \sigma_2 \sigma_3 \sigma_4 \left\{ \mu_1 \mu_2 - \mu_1 \mu_4 + \mu_3 \mu_4 - \mu_3 \mu_2 \right\} \right. \\ \left. + \tilde{c}_4 \left\{ \mu_1 \mu_4 - \mu_1 \mu_2 + \mu_2 \mu_3 - \mu_3 \mu_4 \right\} \right. \\ \left. - \tilde{c}_5 \sigma_1 \sigma_2 \sigma_3 \sigma_4 \left\{ 1 + \mu_1 \mu_2 \mu_3 \mu_4 \right\} \right. \\ \left. + \tilde{c}_6 \sigma_1 \sigma_2 \sigma_3 \sigma_4 \mu_1 \mu_3 \right]. \end{aligned} \quad (4.7)$$

The terms involving the  $\sigma_i$  appear to have the plaquette form associated with Ising gauge fields. The spatial structure of these gauge interactions is made clearer by the transformation in Fig 8. Here, we have collapsed pairs of sites connected by the diagonal links into single sites—we now see that the  $\sigma_i$  can be viewed as residing on the links of a square lattice which is tilted by  $45^\circ$  from the original lattice, and their gauge interactions have the usual form around elementary plaquettes.

The  $\mu_i$  constitute a separate global Ising degree of freedom associated with the breaking of the symmetry of  $90^\circ$  spatial rotations between the horizontal and vertical directions. In the mean-field theory of the deconfined phase, the state with  $\mu_i = 1$  corresponds to the state with dominant spin correlations at the wavevector  $(\pi, q)$  (say). The degenerate partner state with spin correlations at  $(q, \pi)$  is obtained by the state  $\mu_i = (-1)^{i_y}$ , where  $(i_x, i_y)$  are the Cartesian co-ordinates of the site  $i$ .

So the action  $\mathcal{S}_3$  describes a  $Z_2$  gauge theory ( $\sigma$ ) coupled (rather intricately) to an Ising spin field ( $\mu$ ); the  $\mu$  field does not carry a non-zero charge under the  $Z_2$  gauge transformation. The  $Z_2$  gauge theory can undergo a confinement-deconfinement transition (which is related by a duality transformation to the magnetic transition in an Ising model in three dimensions), corresponding to the liberation of spinons upon moving out of the dimer phase. In a different sector, the ordering of the  $\mu$  degrees of freedom leads to the appearance of nematic order, and the breaking of the symmetry of  $90^\circ$  spatial rotations. In the mean-field theory, these two transitions occur at the same point *i.e.* the deconfinement transition is also the point where the spatial rotation symmetry is broken. More generally, the interplay between these two potentially distinct transitions can be addressed by an analysis of fluctuations using the action  $\mathcal{S}_3$ . It does appear possible that the two transitions are not simultaneous, and that there can be a deconfined phase without any broken spatial symmetries; moreover, if there is a simultaneous transition in the two sectors, it is likely to be first order. A more definitive conclusion on these issues must await a complete study of the coupled Ising gauge/Ising spin theory defined by  $\mathcal{S}_3$ . We note that these issues concerning the transition from the confined dimer phase to the deconfined helical SRO phase are somewhat different from earlier deconfinement transitions<sup>23</sup> because here the dimer phase does not break any lattice symmetries.

## V. CONCLUSIONS

The Mott insulator  $\text{SrCu}_2(\text{BO}_3)_2$  is perhaps the only example of a spin gap paramagnet on a strongly frustrated two-dimensional lattice (another example of a two-dimensional paramagnet is  $\text{CaV}_4\text{O}_9$ , but its spin gap is realized by dilution and not frustration). To date, it appears that the spin gap is realized in a simple decoupled dimer ground state discovered originally by Shastry and Sutherland<sup>3</sup>. Here, we undertook a more detailed study of the parameter space of this antiferromagnet, and found that other paramagnetic spin gap states are also possible. One of these was the plaquette state<sup>8</sup>, which appears in a region of weaker frustration and commensurate spin correlations. The other was a more exotic state with “topological order”, deconfined  $S = 1/2$  excitations, and helical spin correlations. The latter state was found to be contiguous to the dimer state, and so not too far from the physically relevant regime: it appears that  $\text{SrCu}_2(\text{BO}_3)_2$  is quite close to the boundary of stability of the dimer phase.

Our results suggest exciting possibilities for materials obtained by doping  $\text{SrCu}_2(\text{BO}_3)_2$  with mobile carriers. It is expected that the helical state will be more amenable to the motion of charge carriers than the dimer state, and so doping may well drive the system into a topologically ordered state. Such a state is a prime candidate for

superconductivity with the exotic properties associated with the proximity of a Mott insulator with deconfined spinons: these include the flux-trapping effect of Senthil and Fisher<sup>33</sup>, and a regime of stable  $hc/e$  vortices<sup>34,35</sup>. An experimental effort to dope  $\text{SrCu}_2(\text{BO}_3)_2$  (or related compounds) therefore appears worthwhile.

## ACKNOWLEDGMENTS

This research was supported by US NSF Grant Nos. DMR 96-23181 (SS) and DMR 97-12391 (JBM).

## APPENDIX:

This appendix will provide a proof of a statement made in Section II A 2 on the nature of the saddle point in the phase with helical LRO: we will analytically show that in the  $(\pi, q)$  and  $(q, \pi)$  LRO phase the link fields obey the following relations:

$$\begin{aligned} Q &= P \\ |R_1| &= |R_2|, \end{aligned} \quad (\text{A1})$$

where  $|Q_i| = Q$ ,  $|P_i| = P$ . The reasoning is the same in the both  $(\pi, q)$  and  $(q, \pi)$  phase, and we will fix our state in the  $(\pi, q)$  phase for simplicity. In this state, the directions of the link fields  $Q_{ij}$  are shown as in Fig 2. The spinon dispersion in this phase can be obtained from the following eigenvalue equation<sup>15</sup> in momentum space:

$$\begin{aligned} \tau^3 D(k) M &= M \tau^3 \hat{\omega}(k) \\ \tau^3 &= \begin{pmatrix} \mathbb{1} & 0 \\ 0 & -\mathbb{1} \end{pmatrix} \\ D(k) &= \begin{pmatrix} \lambda \mathbb{1} & P(k) \\ P^\dagger(k) & \lambda \mathbb{1} \end{pmatrix} \end{aligned} \quad (\text{A2})$$

where  $\mathbb{1}$  is the  $4 \times 4$  unit matrix,  $\hat{\omega}(k)$  is a diagonal matrix of the bosonic eigenenergies,  $M$  is a  $8 \times 8$  matrix whose columns are the eigenvectors of the matrix  $\tau^3 D(k)$  and the diagonal elements of  $\tau^3 \hat{\omega}(k)$  are the corresponding eigenvalues,  $P(k)$  is a  $4 \times 4$  matrix with the following form

$$P(k) = \begin{pmatrix} 0 & iJ_1 Q \sin(k_x) & & & & & & \\ iJ_1 Q \sin(k_x) & 0 & & & & & & \\ -(J_2 R_1/2)e^{-i(k_x - k_y)} & iJ_1 P \sin(k_y) & & & & & & \\ iJ_1 P \sin(k_y) & -(J_2 R_2/2)e^{-i(k_x + k_y)} & & & & & & \\ (J_2 R_1/2)e^{i(k_x - k_y)} & iJ_1 P \sin(k_y) & & & & & & \\ (J_2 R_2/2)e^{i(k_x + k_y)} & & & & & & & \\ 0 & iJ_1 Q \sin(k_x) & & & & & & \\ iJ_1 Q \sin(k_x) & 0 & & & & & & \end{pmatrix}, \quad (\text{A3})$$

and  $\lambda$  is the Lagrange multiplier of the mean-field Hamiltonian which we assume to be independent of lattice site  $i$ . With this assumption, it can be shown<sup>15</sup>

that the eigenvalues occur in pairs with opposite signs  $(\omega_\mu(k), -\omega_\mu(k))$  where  $\mu = 1, \dots, 4$ , and the matrix  $M$  has the form

$$M = \begin{pmatrix} U & -V^* \\ V & U^* \end{pmatrix}, \quad (\text{A4})$$

where the  $U, V$  are  $4 \times 4$  matrices associated with the positive eigenvalues. The  $(\pi, q)$  LRO phase ( $x_i^\alpha \neq 0$ ) occurs at the wavevector  $\vec{k}_{min} = (\pm\pi/2, \pm q/2)$  where the eigenenergy vanishes, ie.  $\omega(\vec{k}_{min}) = 0$ . The two linearly independent eigenvectors associated with  $\vec{k}_1 = (\pi/2, q/2)$  and  $\vec{k}_2 = (\pi/2, -q/2)$  can be shown to be

$$\begin{aligned} \Psi_1 &= (1, ie^{-iq/2}, ie^{-iq/2}, 1, i, -e^{-iq/2}, -e^{-iq/2}, i)e^{i\vec{k}_1 \cdot \vec{r}} \\ \Psi_2 &= (1, ie^{iq/2}, ie^{iq/2}, 1, -i, e^{iq/2}, e^{iq/2}, -i)e^{i\vec{k}_2 \cdot \vec{r}} \end{aligned} \quad (\text{A5})$$

respectively. Substituting  $\Psi_1$  (or  $\Psi_2$ ) into (A2), we have

$$\begin{aligned} \lambda - [J_1(P + Q) \sin(q/2) + J_2 \frac{R_1}{2} \sin(q)] \\ + i[J_1 Q \cos(q/2) + J_2 \frac{R_1}{2} \cos(q)] &= 0 \\ \lambda - [J_1(P + Q) \sin(q/2) + J_2 \frac{R_2}{2} \sin(q)] \\ + i[J_1 Q \cos(q/2) + J_2 \frac{R_2}{2} \cos(q)] &= 0 \end{aligned} \quad (\text{A6})$$

We can easily see that  $R_1 = R_2 = R$  from the above conditions. Also, we find that each saddle-point may be described by purely real  $\langle Q_{ij} \rangle$ . Therefore, we may fix the values of  $\lambda$  and  $q$  in the LRO phase from the above condition.

$$\begin{aligned} J_1(P + Q) \sin(q/2) + J_2 \frac{R}{2} \sin(q) &= \lambda \\ J_1 Q \cos(q/2) + J_2 \frac{R}{2} \cos(q) &= 0 \end{aligned} \quad (\text{A7})$$

To prove  $P = Q$ , we need one additional condition from the saddle-point equations. The mean-field free energy  $E_{MF}$  is a function of  $\lambda, Q, P, R$  and  $x^\alpha(q)$  where these are independent parameters. The large-N solutions of this model are obtained by solving the saddle-point equations which set the derivatives of free energy with respect to these independent variables to be zero. Notice that  $q$  is also an independent parameter. The additional condition we need comes from the saddle-point equation associated with  $q$ . It is given by

$$\frac{\partial E_{MF}}{\partial q} = 0. \quad (\text{A8})$$

The only explicit  $q$  dependence in the free energy is in the bose condensate variables  $x^\alpha(q)$ . This piece of free energy is given by<sup>15</sup>

$$E_x(q) = \sum_{i>j} \frac{J_{ij}}{2} \left[ -Q_{ij} \epsilon_{\sigma\sigma'} x_i^\sigma(q) x_j^{\sigma'}(q) + \text{H.c.} \right], \quad (\text{A9})$$



where  $\epsilon_{\sigma\sigma'}$  is the  $SU(2)$  antisymmetric  $\epsilon$  tensor, and  $\sigma, \sigma' = \uparrow, \downarrow$ . The condensates  $x_i^\sigma(q)$  must be the linear combinations of the eigenvectors  $\Psi_1$  and  $\Psi_2$  associated with the zero mode: this introduces two complex numbers  $c_1, c_2$ , with only the value of  $|c_1|^2 + |c_2|^2$  fixed by the saddle-point equations<sup>15</sup>. Working out the orientation of the condensate at every lattice site over the unit cell, the condensates can be written in the form

$$\begin{aligned} \begin{pmatrix} x_A^\uparrow \\ x_A^\downarrow \end{pmatrix} &= \begin{pmatrix} c_1 + c_2 \\ ic_2^* - ic_1^* \end{pmatrix} \\ \begin{pmatrix} x_B^\uparrow \\ x_B^\downarrow \end{pmatrix} &= \begin{pmatrix} -c_1 e^{-iq/2} - c_2 e^{iq/2} \\ -ic_2^* e^{-iq/2} + ic_1^* e^{iq/2} \end{pmatrix} \\ \begin{pmatrix} x_C^\uparrow \\ x_C^\downarrow \end{pmatrix} &= \begin{pmatrix} -c_1 e^{-iq} - c_2 e^{iq} \\ -ic_2^* e^{-iq} - ic_1^* e^{iq} \end{pmatrix} \\ \begin{pmatrix} x_D^\uparrow \\ x_D^\downarrow \end{pmatrix} &= \begin{pmatrix} c_1 e^{-iq/2} + c_2 e^{iq/2} \\ ic_2^* e^{-iq/2} - ic_1^* e^{iq/2} \end{pmatrix} \end{aligned} \quad (\text{A10})$$

By substituting (A10) into (A9), we can explicitly work out  $E_x(q)$ . It is given by

$$E_x(q) = -[J_1(P + Q) \sin(q/2) + J_2 \frac{R}{2} \sin(q)](|c_1|^2 + |c_2|^2). \quad (\text{A11})$$

Now the saddle-point condition (A8) becomes

$$\frac{\partial E_{MF}}{\partial q} = J_1 \frac{P + Q}{2} \cos(q/2) + J_2 \frac{R}{2} \cos(q) = 0. \quad (\text{A12})$$

Combining (A7) and (A12), we have  $P = Q$ .

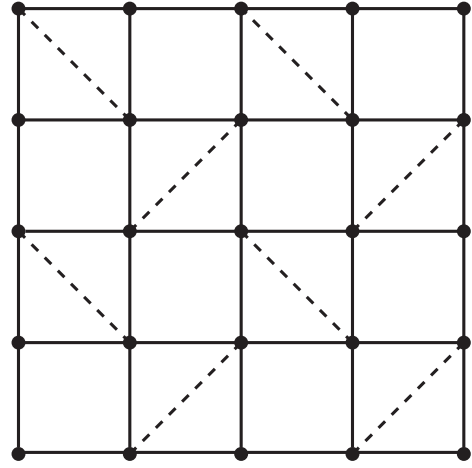


FIG. 1. The Shastry-Sutherland lattice. The exchange  $J_1$  acts between sites separated by the horizontal and vertical links, which the exchange  $J_2$  acts across the diagonal links.

<sup>1</sup> H. Kageyama, K. Yoshimura, R. Stern, N. V. Mushnikov, K. Onizuka, M. Kato, K. Kosuge, C. P. Slichter, T. Goto and Y. Ueda, Phys. Rev. Lett. **82**, 3168 (1999).  
<sup>2</sup> H. Kageyama, M. Nishi, N. Aso, K. Onizuka, T. Yoshihama, K. Nukui, K. Kodama, K. Kakurai, and Y. Ueda, Phys. Rev. Lett. **84**, 5876 (2000).  
<sup>3</sup> B. S. Shastry and B. Sutherland, Physica B **108**, 1069 (1981).  
<sup>4</sup> S. Miyahara and K. Ueda, Phys. Rev. Lett. **82**, 3701 (1999).  
<sup>5</sup> M. Albrecht and F. Mila, Europhys. Lett. **34**, 145 (1996).  
<sup>6</sup> Z. Weihong, C. J. Hamer and J. Oitmaa, Phys. Rev. B **60**, 6608 (1999).  
<sup>7</sup> E. Müller-Hartmann, R. R. P. Singh, C. Knetter and G. S. Uhrig, Phys. Rev. Lett. **84**, 1808 (2000).  
<sup>8</sup> A. Koga and N. Kawakami, Phys. Rev. Lett. **84**, 4461 (2000).  
<sup>9</sup> C. Knetter, A. Bühler, E. Müller-Hartmann, and G. S. Uhrig, Phys. Rev. Lett. **85**, 3958 (2000).  
<sup>10</sup> D. Carpentier and L. Balents, cond-mat/0102218.  
<sup>11</sup> G. Misguich, Th. Jolicoeur, and S. M. Girvin, cond-mat/0102377.

<sup>12</sup> N. Read and S. Sachdev, Phys. Rev. Lett. **66**, 1773 (1991).  
<sup>13</sup> R. Jalabert and S. Sachdev, Phys. Rev. B **44**, 686 (1991).  
<sup>14</sup> S. Sachdev and N. Read, Int. J. Mod. Phys. B **5**, 219 (1991).  
<sup>15</sup> S. Sachdev, Phys. Rev. B **45**, 12377 (1992).  
<sup>16</sup> C. H. Chung, J. B. Marston, and R. H. McKenzie, cond-mat/0012216.  
<sup>17</sup> S. Sachdev and R. Jalabert, Mod. Phys. Lett. B **4**, 1043 (1990).  
<sup>18</sup> O. P. Sushkov, J. Oitmaa, and Z. Weihong, cond-mat/0007329.  
<sup>19</sup> N. Read and S. Sachdev, Phys. Rev. Lett. **62**, 1694 (1989).  
<sup>20</sup> N. Read and S. Sachdev, Phys. Rev. B **42**, 4568 (1990).  
<sup>21</sup> E. Fradkin and S. Shenker, Phys. Rev. D **19**, 3682 (1976).  
<sup>22</sup> X. G. Wen, Phys. Rev. B **44**, 2664 (1991).  
<sup>23</sup> S. Sachdev and M. Vojta, J. Phys. Soc. Japan **69**, Suppl. B, 1 (2000).  
<sup>24</sup> T. Senthil and M. P. A. Fisher, Phys. Rev. B **62**, 7850 (2000).  
<sup>25</sup> D. Rokhsar and S. Kivelson, Phys. Rev. Lett. **61**, 2376 (1988).  
<sup>26</sup> N. Read and B. Chakraborty, Phys. Rev. B **40**, 7133 (1989).  
<sup>27</sup> G. Misguich and C. Lhuillier, cond-mat/0002170.  
<sup>28</sup> R. Moessner and S. Sondhi, cond-mat/0007378.  
<sup>29</sup> S. Sachdev and N. Read, Phys. Rev. Lett. **77**, 4800 (1996).  
<sup>30</sup> E. Fradkin and S. Kivelson, Mod. Phys. Lett. B **4**, 229 (1990).  
<sup>31</sup> W. Zheng and S. Sachdev, Phys. Rev. B **40**, 2704 (1989).  
<sup>32</sup> M. S. L. du Croo de Jongh, J. M. J. van Leeuwen, W. van Saarloos, cond-mat/0002116.  
<sup>33</sup> T. Senthil and M. P. A. Fisher, Phys. Rev. Lett. **86**, 292 (2001).  
<sup>34</sup> S. Sachdev, Phys. Rev. B **45**, 389 (1992).  
<sup>35</sup> N. Nagaosa and P. A. Lee, Phys. Rev. B **45**, 966 (1992).

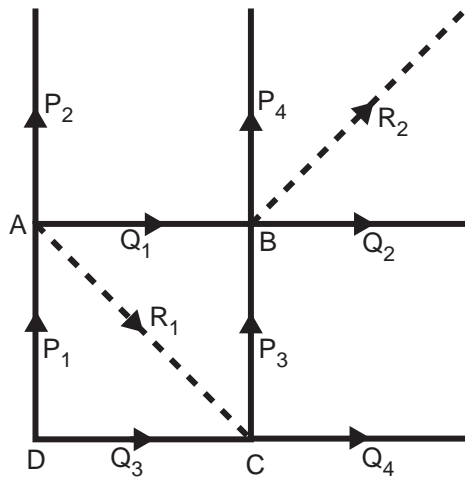


FIG. 2. The four sites of the unit cell (labeled A, B, C and D), and the 10 link variables  $Q_{ij}$ .

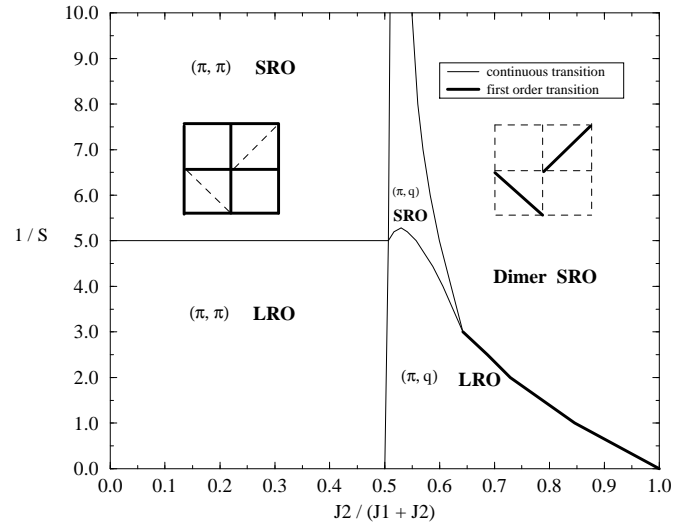


FIG. 3. Large  $N$  phase diagram of the  $Sp(N)$  Shastry-Sutherland model, Eq. 1.1, as a function of  $J_2/(J_1 + J_2)$  and  $1/S$ . The five phases are described in Section II. The LRO phases break spin-rotation symmetry: the spin order is collinear and commensurate in the  $(\pi, \pi)$  LRO phase, and helical and incommensurate in the  $(\pi, q)$  LRO phase. The SRO phases preserve spin rotation invariance. In the  $(\pi, \pi)$  SRO only the horizontal and vertical  $Q_{ij}$  are non-zero in the large  $N$  theory—fluctuations lead to broken translational symmetry in one of the states shown in Fig 6. (A state with co-existing  $(\pi, \pi)$  LRO and plaquette order is also allowed by the theory<sup>17</sup> beyond the large  $N$  limit (not shown above), and there is evidence that this occurs on a frustrated square lattice antiferromagnet<sup>18</sup>.) The dimer phase has only the diagonal  $Q_{ij}$  non-zero in the large  $N$  theory. The  $(\pi, q)$  SRO phase has all the  $Q_{ij}$  non-zero: this phase has topological order and deconfined spinons.

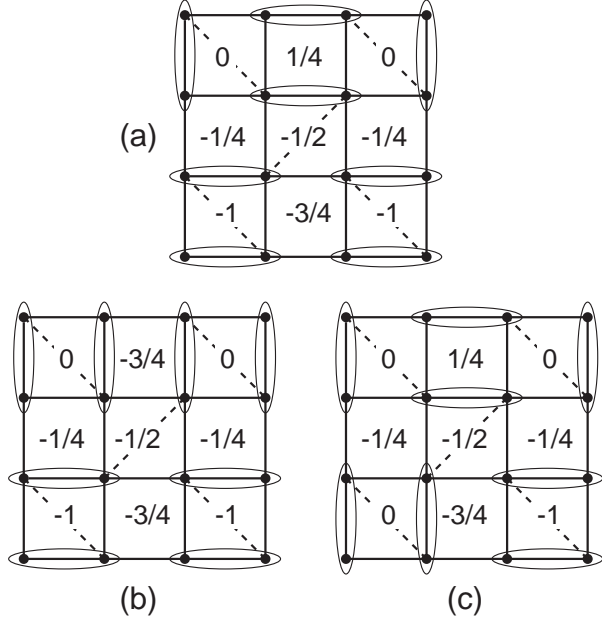


FIG. 4. Three states of the Hilbert space of the quantum dimer model. There are off-diagonal matrix elements in the effective Hamiltonian which connect state (a) to state (b), and state (a) to state (c), by a resonance between pairs of horizontal and vertical dimers around a plaquette. The latter matrix element differs from the former because only the latter has a diagonal link across the resonating plaquette. Also shown are the corresponding values of the heights,  $h_a$ , on the sites of the dual lattice.

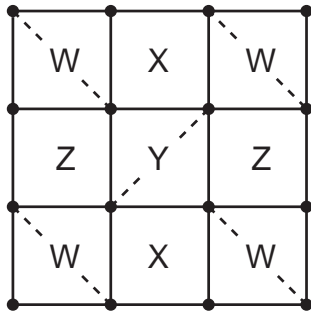


FIG. 5. The four dual sublattices upon which the height offsets take the values  $\zeta_W = 0$ ,  $\zeta_X = 1/4$ ,  $\zeta_Y = 1/2$ , and  $\zeta_Z = 3/4$ .

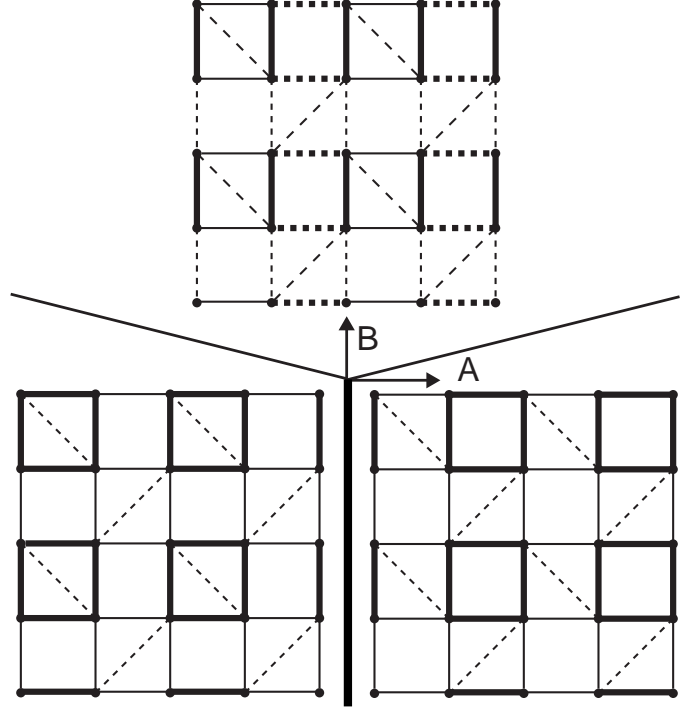


FIG. 6. Phase diagram of (3.6) as a function of the parameters  $A$  and  $B$ ; this model describes fluctuations in the  $(\pi, \pi)$  SRO phase of Fig 3. The thick line is a first order transition, while the thin lines are second order. The plaquette and spin-Peierls states are shown, with the different line-styles representing distinct values of  $\langle \mathbf{S}_i \cdot \mathbf{S}_j \rangle$  across the links.

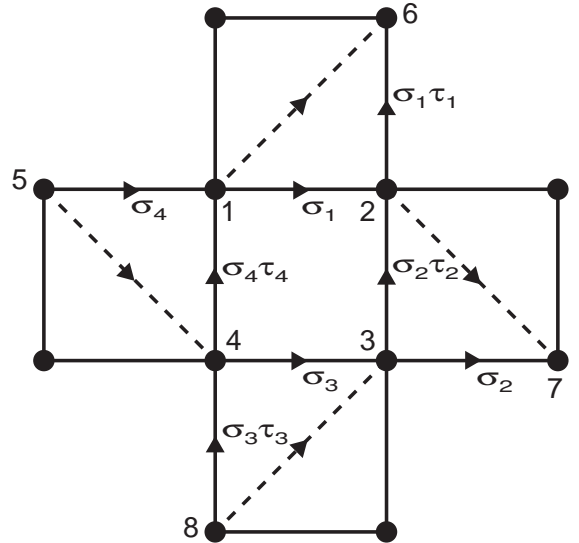


FIG. 7. A section of the Shastry-Sutherland lattice. We have labeled sites around the central plaquette to enable the discussion in Section IV of the various terms in the  $Z_2$  gauge theory of the transition from the dimer state to the  $(\pi, q)$  SRO phase with spinon deconfinement.

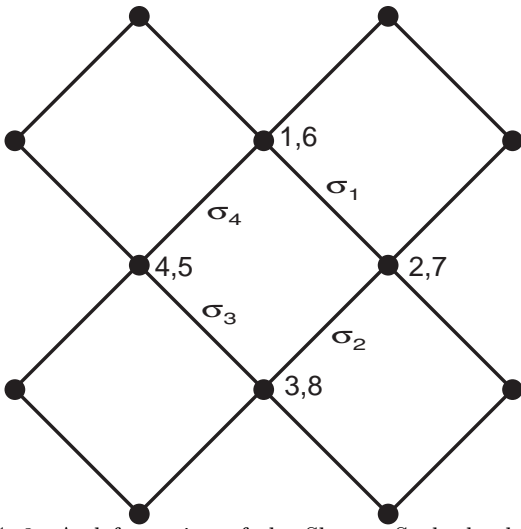


FIG. 8. A deformation of the Shastry-Sutherland lattice which exposes the structure of the  $Z_2$  gauge theory. Pairs of sites across a diagonal bond have been compressed into a single site. Four of the sites carry pairs of sites labels, corresponding to the original site numbers in Fig 7. The  $Z_2$  Ising gauge fields on some of the links are indicated, with a notation corresponding to the degrees of freedom in Fig 7.